Available online at www.sciencedirect.com
ScienceDirect
Journal of the European Ceramic Society 31 (2011) 1525–1531
www.elsevier.com/locate/jeurceramsoc

Microcracking of high zirconia refractories after t → m phase transition during cooling: An EBSD study

Arnaud Sibil [a], Thierry Douillard [a], Cyril Cayron [b], Nathalie Godin [a], Mohamed R'mili [a], Gilbert Fantozzi [a,*]

[a] Université de Lyon, INSA-Lyon, UMR CNRS 5510, 69621 Villeurbanne, France
[b] CEA, LITEN, DETH, Minatec, 38054 Grenoble, France

Received 23 December 2010; received in revised form 14 February 2011; accepted 22 February 2011
Available online 31 March 2011

Abstract

High zirconia refractories are composed of a zirconia skeleton surrounded by an intergranular glassy phase. In these materials, zirconia undergoes up to two successive phase transitions during the manufacturing process, c → t then t → m. This leads, after complete cooling, to the formation of microcracks.

Preliminary observations have enabled to identify the mechanism mostly responsible for the observed microcracking. In particular, SEM imaging emphasizes the link between the positions of cracks and the presence of distinct crystallographic domains.

Thus, our work focuses on the arrangement of the monoclinic and tetragonal domains in zirconia dendrites. The assessment by XRD of the thermal expansion coefficients of zirconia at the lattice scale and the analysis of EBSD maps show that cracking is produced by the thermal expansion mismatch between groups of crystallographic variants. The further reconstruction of both cubic and tetragonal – in the case of a presence of monoclinic zirconia at room temperature – parent grains enables to determine the impact of each transition on the final microstructure and the generated microcracking.

Keywords: Electron backscattering diffraction (EBSD); Zirconia; Refractories; Martensitic phase transformation

1. Introduction

High zirconia fused-cast refractories are composed of a zirconia skeleton made of dendrites surrounded by an intergranular glassy phase.[1–5] During their manufacturing process, by casting from high temperatures (2700 °C), the zirconia undergoes up to two successive phase transformations: cubic to tetragonal (c → t at 2370 °C for pure zirconia) and tetragonal to monoclinic (t → m at around 1080 °C for the considered material in this study). The glassy phase is important to obtain such massive monoclinic zirconia materials because it prevents from extensive cracking during this last transition and it accommodates the internal stresses developed by the associated increase of volume[6,7] (3–5%). Preserving their integrity, these materials nevertheless present cracks – that do not compromise their properties in service – at different scales after complete cooling. Several mechanisms can be pointed out to explain the observed microcracking.[4,5] For instance, for the t → m phase transition, the supposed thermal expansion (TE) mismatch between glassy phase and zirconia during cooling or the presence of heterogeneities such as the porosity sizes or the variations of composition of the glassy phase could be proposed. As microcracking is mainly observed within zirconia, our work has been oriented by the possible impact of the thermal expansion anisotropy of the zirconia lattice.[8] A coherent picture of the state of the art in zirconia crystallography and its phase transformation is presented by Green et al.[9] Indeed, each phase transformation can lead to the formation of different variants. For the c → t transformation, only three correspondences are possible, according to whether the tetragonal c axis replaces the a, b or c cubic axis. Concerning the t → m transition, that is of martensitic type, six correspondences (see Table 1) and their associated orientation relationships (ORs) are reported by Kelly and Francis Rose[10] leading to four monoclinic variants

* Corresponding author.
E-mail address: gilbert.fantozzi@insa-lyon.fr (G. Fantozzi).

0955-2219/$ – see front matter © 2011 Elsevier Ltd. All rights reserved.
doi:10.1016/j.jeurceramsoc.2011.02.033

Table 1
The different ORs as reported by Kelly et al.[10]

OR A-1	OR B-1	OR C-1
$(0\,0\,1)_m//(0\,1\,0)_t$	$(0\,0\,1)_m//(1\,0\,0)_t$	$(0\,0\,1)_m//(0\,0\,1)_t$
$[1\,0\,0]_m//[0\,0\,1]_t$	$[1\,0\,0]_m//[0\,1\,0]_t$	$[1\,0\,0]_m//[1\,0\,0]_t$
$[0\,1\,0]_m//[1\,0\,0]_t$	$[0\,1\,0]_m//[0\,0\,1]_t$	$[0\,1\,0]_m//[0\,1\,0]_t$
OR A-2	**OR B-2**	**OR C-2**
$(1\,0\,0)_m//(0\,0\,1)_t$	$(1\,0\,0)_m//(0\,1\,0)_t$	$(1\,0\,0)_m//(1\,0\,0)_t$
$[0\,0\,1]_m//[0\,1\,0]_t$	$[0\,1\,0]_m//[0\,0\,1]_t$	$[0\,0\,1]_m//[0\,0\,1]_t$
$[0\,1\,0]_m//[1\,0\,0]_t$	$[0\,0\,1]_m//[1\,0\,0]_t$	$[0\,1\,0]_m//[0\,1\,0]_t$

per correspondence. However, the phenomenological theory of martensite crystallography[10,11] shows that the ABC correspondence – where the a, b and c axes of tetragonal zirconia become respectively the a, b and c axes of monoclinic zirconia – is the most preferable one on a energetic point of view and therefore must be the most often met. Following these crystallographic considerations, it can be assumed that disorientations between variants can lead to a thermal expansion mismatch at their interface leading to internal stresses that may be released by cracking. Thus cracks location would be linked to the crystallographic domains. Preliminary observations have been performed to confirm this hypothesis.

While the mechanism of microcracking has been clearly identified, there is still a need to go further in the understanding of the cracking. The objective of this paper is to show precisely the link between the arrangement of the variants and the implantation of the cracks. As the selected material is differing from those in the literature by its crystallographic history and as there is no data concerning the thermal expansion coefficients of the tetragonal structure, these coefficients were assessed by XRD and Rietveld's refinement method[12] for both monoclinic and tetragonal zirconia at the lattice scale. The obtained values were treated to assess the thermal expansion mismatch between variants. Then, the acquisition and analysis of an *Electron BackScatter Diffraction* (EBSD) map of this non-conductive material shows the rules that govern cracking in the dendrites. In particular, the two ways of propagation observed by SEM are discussed. Finally, via the reconstruction of both cubic and tetragonal – in the case of a presence of monoclinic zirconia at room temperature – parent grains as for other structures and transitions,[13,14] the impact of each phase transition on the global microcracking process is emphasized.

2. Experimental procedure

In this study, two high zirconia fused-cast materials supplied by Saint-Gobain CREE were considered, differing from the presence or the absence of a stabilizing agent within zirconia. The microstructure characteristics (mean diameter of the dendrites, thickness of the intergranular glassy phases) are similar. The material 1 contains 94 wt.% of pure monoclinic zirconia and 6 wt.% of a glassy phase and it undergoes the t → m transition. On the contrary, material 2 contains 7 mol.% yttria stabilized zirconia and remains tetragonal at room temperature.

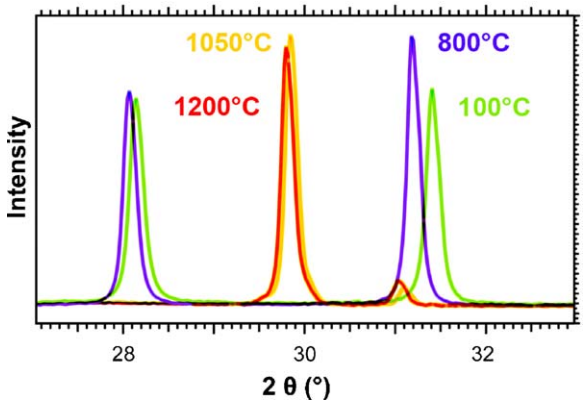

Fig. 1. Zoom from extended scans in temperature for both monoclinic and tetragonal states of material 1.

2.1. XRD diffraction and TE coefficients determination

In order to avoid any bias of measurement, the glassy phase was removed from the samples by a chemical attack with fluorhydric acid. These samples were then reduced into powder by the mean of a planetary milling to prevent from internal stresses effect. For this operation, rotation speed was set to 300 rpm, duration to 30 min and material/balls volume ration to 0.5. The average diameter of the obtained particles was determined at 150 nm by laser granulometry.

The assessment of the thermal expansion coefficients at the lattice scale was performed using a Bruker D8 Discover X-ray diffractometer equipped with a high temperatures furnace. An X-ray tube with a copper anode ($K\alpha_1 = 0.1540562$ nm) was used as generator. $K\alpha_2$ transition X-rays were removed by a primary monochromator of the Johansson type. Extended scans (2θ from 10 to 120°) were acquired at different temperatures by a 3° linear detector for both monoclinic and tetragonal structures (Fig. 1). They were preceded by a dwell of 10 min to ensure that the temperature is homogeneous within the furnace. The scan step and the scan speed were respectively set to 0.045° and 1.5 s per sample, conducting to a duration of around an hour for each scan.

The scans were processed through the software TOPAS (Bruker AXS). In particular, the lattice parameters were determined for each temperature using the integrated Rietveld's refinement method. Through the comparison of these parameters versus temperature, the different thermal expansion coefficients were calculated for both structures.

2.2. EBSD acquisition and treatments

Since the studied material is insulating, SEM imaging conditions had to be found to ensure a correct contrast on the diffraction patterns. The samples were cut by diamond grinding to the following dimensions: 10 mm × 10 mm × 0.8 mm. They were prepared by conventional diamond polishing down to 1 μm completed by a vibratory polishing with colloidal silica (0.1 μm).

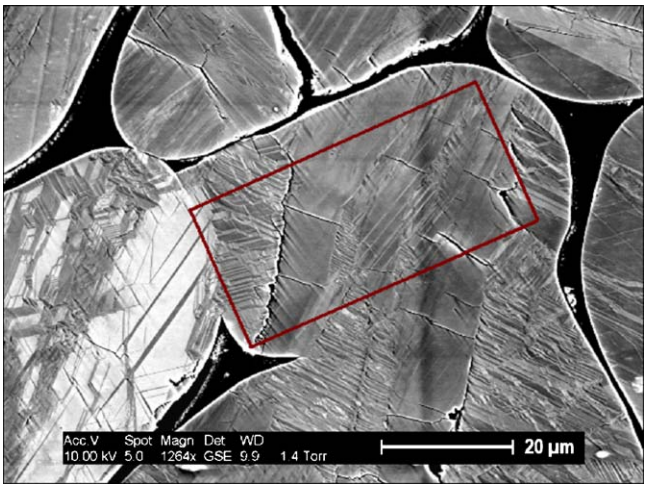

Fig. 2. Area analysed by EBSD.

Two EBSD maps have been acquired on a ZEISS SUPRA™ 55 VP SEM equipped with an Oxford/HKL EBSD system. For the material 1, the scanned area (width and height respectively 24 and 50 μm) is entirely contained within a zirconia dendrite, i.e. there is no overlapping on the glassy phase (Fig. 2). The EBSD mapping was done with an accelerating voltage of 20 kV, an air pressure of 20 Pa and with a step of 40 nm. The step size was selected according to the size of the previously observed monoclinic domains (Fig. 3) so as to get a good indexing rate. For the material 2, the scanned area (width and height respectively 985 and 740 μm) includes approximately 200 dendrites surrounded by the intergranular glassy phase. The mapping step was increased to 0.8 μm. Both samples were tilted to 70°. The available environmental mode has been of a great interest in allowing not to use any carbon coating in contrary to standard procedures for ceramics reported in the literature.[15]

Data were processed with Oxford/HKL Channel 5 software suite for indexation and de-noising of the map. The reconstruction of parent grains was performed with ARPGE software[16] and is presented in paper to be published.[17]

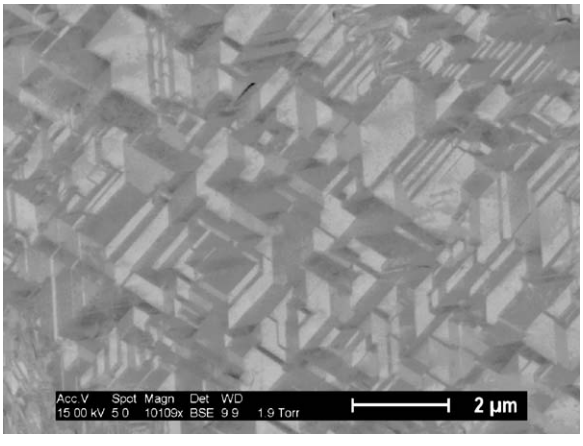

Fig. 3. Submicronic monoclinic domains.

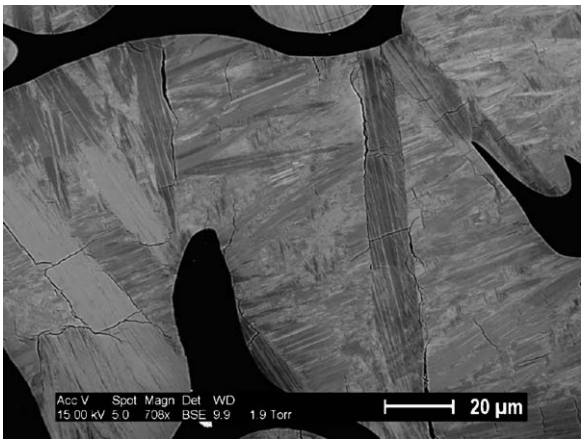

Fig. 4. SEM imaging showing the monoclinic domains and the location of cracks.

3. Preliminary observations

3.1. SEM imaging

SEM investigations on material 1 have been performed on a FEI ESEM-FEG XL30 SEM using a backscattered electron detector in low vacuum environment under a water pressure of 250 Pa. It shows that the localisation and orientations of the cracks are correlated to the borders of the monoclinic domains that are emphasized by contrasts of orientations (see Fig. 4). It can be noted that cracks do not propagate randomly but in two particular modes: whether (a) they are located at the interface of two monoclinic domains or (b) they are propagated perpendicularly to two domains, crossing partially or entirely other domains between them. In this last case, the crossed domains form a picture similar to those formed by twins in martensite.

3.2. Acoustic emission monitoring

Additional elements plead in favour of thermal expansion mismatch as mechanism responsible for microcracking. Acoustic emission monitoring on material 1[18,19] has been performed during cooling from 1200 °C (see Fig. 5). The refractory sample (80 mm × 12.5 mm × 8 mm) was held in a furnace by two zirconia waveguides (Ø 8 mm × 210 mm) located on each side of his length. Acoustic signals were conducted through these waveguides and detected by two sensors linked to pre-amplifiers and an acquisition system. Thanks to this configuration, a linear localisation of the signals was performed so as to ignore noise. The results show that there is no activity above the glassy phase transition temperature except for the t → m phase transition (Fig. 5(a)). This could be explained by the behaviour of the glassy phase that accommodates the evolutions of the zirconia skeleton. On the contrary, the energy released by signals increases in an significant way as the temperature decreases, indicating that cracking is more and more severe (Fig. 5(b)). Local strain due to thermal expansion mismatch thus logically raises with the decrease of temperature until it reaches the ultimate strength for the considered temperature. Considering for instance a thermal expansion mismatch of $6 \times 10^{-6}\,^{\circ}C^{-1}$

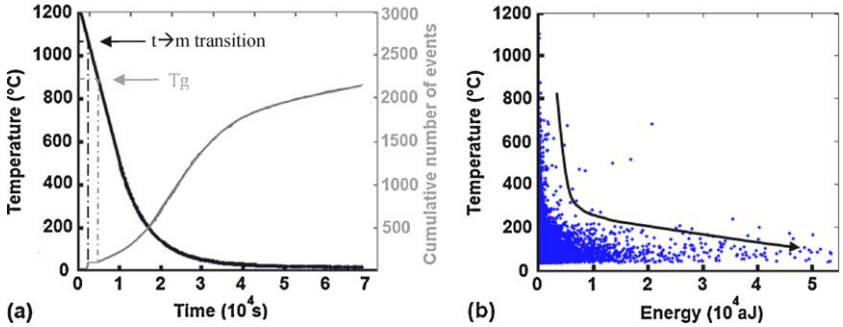

Fig. 5. Acoustic emission monitoring during cooling: (a) global activity and (b) increase of the energy at low temperatures.

between two variants, a cooling down to 200 °C would lead to a strain of about 0.25% for each variant (one variant in traction, the second variant in compression). This chosen value of TE mismatch seems reasonable taking into account the values following the crystallographic axes of monoclinic zirconia reported in literature,[8] 8, 3 and $14 \times 10^{-6}\,°C^{-1}$ respectively following the a, b and c monoclinic axes. It leads to a strain that exceeds the tensile ultimate strain assessed by 4 points flexural tests for low temperatures, from 800 °C down to room temperature, so cracking can be explained by this way.

4. Results and discussion

Couples of XRD scans have been performed at 100 °C and 800 °C during heating for the monoclinic structure and at 1200 °C and 1050 °C during cooling for the tetragonal structure. The assessed lattice parameters of zirconia and the deduced TE coefficients at the lattice scale are presented in Table 2. The values corresponding to the monoclinic state, 8.2, 2.9 and $12.7 \times 10^{-6}\,K^{-1}$ respectively following the a, b and c monoclinic axes, are closed to those reported in the literature for baddeleyite which is a compound frequently used to characterize the properties of monoclinic zirconia. These expected differences are significant and will play an important role by allowing the development of thermal expansion mismatch at the interface of disoriented variants, as it will be pointed out in the following. In addition, a notable difference is also observed following the tetragonal axes. A similar mechanism is therefore also able to occur at higher temperatures in presence of different tetragonal domains within a zirconia dendrite; however, considering the weaker value of the Young's modulus of tetragonal zirconia and the higher value of strength in this range of temperatures, this may conduct only to weak internal stresses prone to be accommodated without microcracking.

Table 2
(a) Lattice parameters versus temperature. (b) Deduced TE coefficients for both monoclinic and tetragonal structures.

	Lattice parameters (Å)		
	a	*b*	*c*
(a)			
100 °C	5.1511	5.2078	5.3220
800 °C	5.1808	5.2183	5.3693
1050 °C	3.6306		5.2591
1200 °C	3.6348		5.2678
	TE coefficients ($\times 10^{-6}\,°C^{-1}$)		
	a	*b*	*c*
(b)			
$Zr0_2m$	8.2	2.9	12.7
$Zr0_2t$	7.7		11.0

The acquired EBSD map presents a satisfactory indexing rate with almost 85% of the area indexed. The remaining percentage is due to the topography associated to cracks and to the joining plans between variants that generates diffuse diffraction. The map has been processed in an iterative way so as to suppress the un-indexed points by affecting the orientation of most of their neighbours. The simplified map is presented in Fig. 6(a). Twelve variants have been found and numbered. Considering that the variants resulting from the same OR share the same monoclinic c axis, it is possible to gather them into groups in calculating the coordinates of this axis in the coordinates system of the sample $\{X, Y \text{ and } Z\}$, Z being the normal vector to the analysed surface. This operation has been performed using the three combined Euler's rotations following Euler's angles φ_1, Φ, φ_2 leading to the rotation matrix $R = R_Z(\varphi_1)R_X(\phi)R_Z(\varphi_2)$ according to:

$$R_z(\varphi_1) = \begin{bmatrix} \cos(\varphi_1) & -\sin(\varphi_1) & 0 \\ \sin(\varphi_1) & \cos(\varphi_1) & 0 \\ 0 & 0 & 1 \end{bmatrix} \quad (1)$$

$$R_x(\phi) = \begin{bmatrix} 1 & 0 & 0 \\ 0 & \cos(\phi) & -\sin(\phi) \\ 0 & \sin(\phi) & \cos(\phi) \end{bmatrix} \quad (2)$$

$$R_z(\varphi_2) = \begin{bmatrix} \cos(\varphi_2) & -\sin(\varphi_2) & 0 \\ \sin(\varphi_2) & \cos(\varphi_2) & 0 \\ 0 & 0 & 1 \end{bmatrix} \quad (3)$$

The Euler's angles and the calculated coordinates of the monoclinic c axis are presented for each variant in Table 3. It shows that the 12 variants can be regrouped into three quadruplets sharing a common c axis: {1,2,3,4}, {5,6,7,8} and {9,10,11,12}.

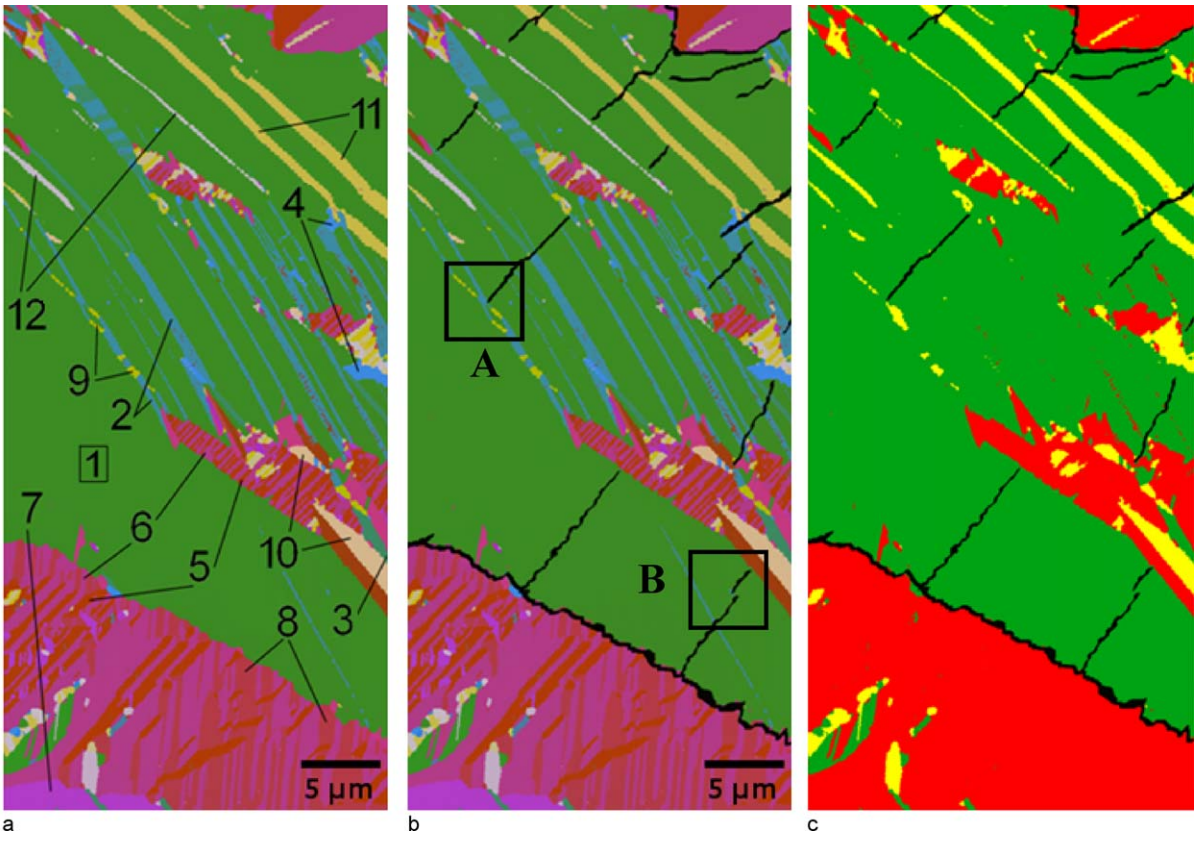

Fig. 6. EBSD map of the analysed area. (a) Numbering of the 12 variants. (b) Position of the cracks. (c) Colouring of the 3 tetragonal domains according to colours of Table 3.

The reconstruction of the tetragonal parent grains confirms this result and indicates that these quadruplets result from the ABC-2 correspondence of three distinct tetragonal domains. It is thus now possible to map the tetragonal domains by colouring the quadruplets of variants. In order to link the cracking with the arrangement of the monoclinic and tetragonal domains, the cracks observed by SEM were added on a map presenting the monoclinic variants (Fig. 6(b)) and on a map showing the tetragonal domains (Fig. 6(c)). It can be noticed that cracks propagate into two modes: either they propagate along the tetragonal domains or they crossed a tetragonal domain almost perpendicularly to the neighbouring domains. Moreover, they are systematically initiated at the interface of two tetragonal domains. This is in adequacy with the phenomenological theory of martensite applied to zirconia which predicts the formation of all the four variants to accommodate the shear component of the t → m transition, pushing back the shear stresses outside the transformed region. With regard to the propagation of cracks, the comparison of maps Fig. 6(b) and (c) shows that cracking within a tetragonal domain can be stopped or deviated by the presence

Table 3
Euler's angles of the 12 indexed variants and the coordinates of the c_m axis of each quadruplet.

	Euler angles (°)			c_m coordinates		
Variants	φ1	Φ	φ2	X	Y	Z
1	42.7	98	49.3	0.67	-0.73	-0.13
2	42.4	97	229.1			
3	43.8	96.2	138.8			
4	42.7	98	318			
5	124.2	41.2	10.9	0.54	0.38	0.74
6	125.3	41.6	190.2			
7	125.2	42	280.6			
8	125.6	39.9	100			
9	138.8	130.5	10	0.51	0.58	-0.63
10	143.2	128.3	197.2			
11	141.2	129.7	102.7			
12	137.1	130.2	279.6			

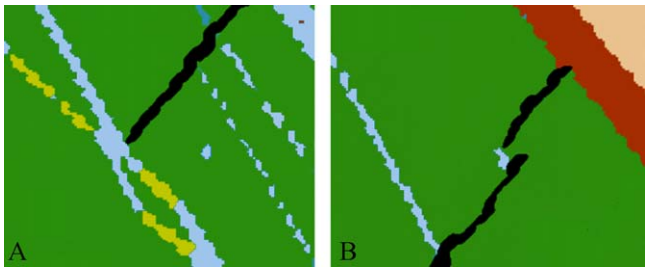

Fig. 7. Detail of zones A and B of Fig. 5(b). Blue variant has been cleared up for better visualization. (For interpretation of the references to color in this figure legend, the reader is referred to the web version of the article.)

of one of the other variants of the corresponding quadruplet. Examples are given in Fig. 6(b), detailed zones are presented in Fig. 7. This seems to indicate that the crossing of another variant involves a large quantity of energy. However it is possible as seen in Fig. 6(b) where tetragonal green and yellow domains are alternatively crossed on the top of the map.

One can notice that the three c_m axes of the three quadruplets are perpendicular each other (Table 3). They correspond to the ⟨1 0 0⟩ axes of a parent cubic phase. A further reconstruction of the cubic parent grains with ARPGE confirms that the three tetragonal domains presented here result from the same cubic domain above 2400 °C. Indeed, the reconstruction of a wider zone containing about 15 dendrites surrounded by glassy phase shows that secondary dendrites belonging to the same primary millimetric-length dendrite share the same cubic orientation.[17] Thus, the whole history of a zirconia dendrite has been determined. It has initially a unique cubic orientation which gives birth to the 3 corresponding tetragonal domains (as observe in this extended map). Then, the t → m transition occurs mainly following the correspondence ABC-2. As cracking does not occur between the variants within a tetragonal domain, it is therefore not a direct consequence of the t → m transition but an indirect consequence of the c → t transition that takes place at higher temperatures. In fact, cracking is only observed at low temperatures within monoclinic zirconia because of the glassy state of the glassy phase and the need of an important gap of temperature to activate the thermal expansion mismatch.

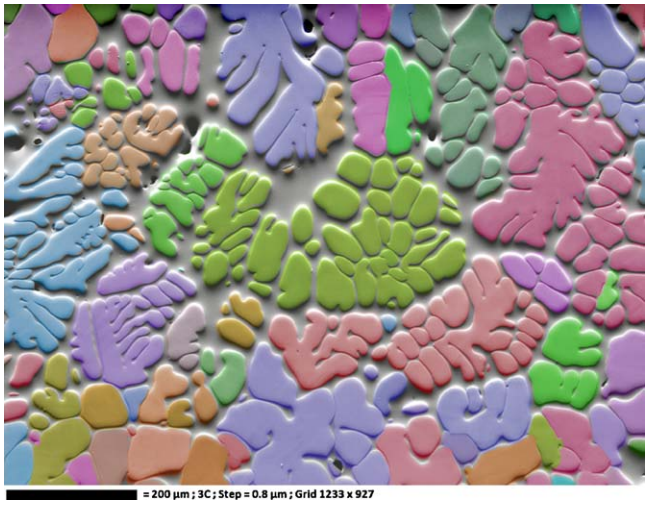

Fig. 8. EBSD map of the analysed area of material 2.

The acquisition of an EBSD map on material 2 (Fig. 8) and its analysis consolidates these results. This second material, contrary to the previous one, does almost not present any microcracks. In addition, it produces only a few signals of acoustic emission during cooling (less than 100 signals against around 55,000 signals for the material 1, in the same experimental settings). This can be explained by a singular distribution of the crystallographic orientations: the EBSD map shows that every dendrites contain a single crystallographic domain. Moreover, primary and secondary dendrites share the same orientation. Thus, no thermal expansion mismatch can operate within the dendrites and consequently no microcracking is generated.

5. Conclusion

This study emphasizes the impact of the thermal expansion mismatch between monoclinic variants on the formation of cracks within zirconia. In particular, it is shown that cracking operates at the interface of the prior tetragonal grains, which form quadruplets of monoclinic variants resulting from the same t → m correspondence. This is in agreement with the phenomenological theory of martensite crystallography applied to zirconia which envisages the creation of quadruplets that adapt the shear components of the transformation. This observation can be performed easily in gathering the variants of a common quadruplet by calculating the monoclinic c axis coordinates for each variant. However the reconstruction of the tetragonal parent grains enables to go further in the analysis in revealing that all quadruplets result from a different tetragonal domain at higher temperature, so that cracks are initiated at the interface of these tetragonal domains. For the t → m transition, correspondence ABC-2 which is described as one of the most energetically favourable correspondence is found. Cracking was shown not to be a direct consequence of the t → m transition but finds its origin in the c → t transition which generates distinct tetragonal domains. It operates at the monoclinic state because of the differences between the thermal expansion coefficients at the lattice scale that are much higher than in the tetragonal state.

These observations are confirmed by the analysis of an EBSD map on a material in which zirconia remains tetragonal at room temperature. As primary and secondary dendrites share the same crystallographic orientation, no microcracking is generated within zirconia.

Acknowledgements

The authors wish to thank the French Ministry of Economy, Finance, and Industry for their financial support (ANR NOREV) and Saint Gobain CREE (Cavaillon, France) for their technical collaboration. We are also grateful to Dr S. Sao-Jao form the Ecole des Mines de Saint-Etienne, UMR CNRS 5146, for providing an EBSD map.

References

1. Madi K, Forest S, Boussuge M, Gailliègue S, Lataste E, Buffière JY, et al. Finite element simulations of the deformation of fused-cast refractories based on X-ray computed tomography. *Comput Mater Sci* 2007;**39**: 224–9.
2. Lataste E, Erauw JP, Olagnon C, Fantozzi G. Microstructural and mechanical consequences of thermal cycles on a high zirconia fuse-cast refractory. *J Eur Ceram Soc* 2009;**29**:587–94.
3. Yeugo Fogaing E, Huger M, Gault C. Elastic properties and microstructure: study of two fused cast refractory materials. *J Eur Ceram Soc* 2007;**27**:1843–8.
4. Patapy C, Gault C, Huger M, Chotard T. Acoustic characterization and microstrucrure of high zirconia electrofused refractories. *J Eur Ceram Soc* 2009;**29**:3355–62.
5. Sibil A, Erauw JP, Cambier F, R'Mili M, Godin N, Fantozzi G. Study of damage of high zirconia fused-cast refractories by measurement of Young's modulus. *Mater Sci Eng A* 2009;**521–522**:221–3.
6. Deville S, Guénin G, Chevalier J. Martensitic transformation in zirconia: Part I. Nanometer scale prediction and measurement of transformation induced relief. *Acta Mater* 2004;**52**:5697–707.
7. Kriven WM. Martensitic toughening of ceramics. *Mater Sci Eng A* 1990;**127**:249–55.
8. Bayer G. Thermal expansion anisotropy of oxide compounds. *Proc Br Ceram Soc* 1973;**22**:39–53.
9. Green DJ, Hannink RHJ, Swain MV. *Transformation toughening of ceramics*. Florida: CRC Press; 1989. p. 17–55.
10. Kelly PM, Francis Rose LR. The martensitic transformation in ceramics—its role in transformation toughening. *Prog Mater Sci* 2002;**47**:463–557.
11. Shibata-Yanagisawa M, Kato M, Seto H, Ishizawa N, Mizutani N, Kato M. Crystallographic analysis of the cubic-to-tetragonal phase transformation in the ZrO_2–Y_2O_3 system. *J Am Ceram Soc* 1987;**70**:503–9.
12. Rietveld HM. A profil refinement method for nuclear and magnetic structures. *J Appl Cryst* 1969;**2**:65–71.
13. Gey N, Humbert M. Specific analysis of EBSD data to study the $\alpha \rightarrow \beta$ phase transformation. *J Mater Sci* 2003;**38**:1289–94.
14. Cayron C, Artaud B, Brittet L. Reconstruction of parent grains from EBSD data. *Mater Charact* 2006;**57**:386–401.
15. Faryna M. TEM and EBSD comparative studies of oxide-carbide composites. *Mater Chem Phys* 2003;**81**:301–4.
16. Cayron C. ARPGE: a computer program to automatically reconstruct the parent grains from electron backscatter diffraction date. *J Appl Cryst* 2007;**40**:1183–8.
17. Cayron C, Douillard T, Sibil A, Sao-Jao S, Fantozzi G. Reconstruction of the cubic and tetragonal parent grains from electron backscatter diffraction maps of monoclinic zirconia. *J Am Ceram Soc* 2010;**93**:2541–4.
18. Beattie AG. Acoustic emission, principles and instrumentation. *J Acoust Emission* 1983;**2**:95–128.
19. Moevus M, Rouby D, Godin N, R'Mili M, Reynaud P, Fantozzi G, et al. Analysis of damage mechanisms and associated acoustic emission in two SiC_f/[Si-B-C] composites exhibiting different tensile behaviours. Part II: Unsupervised acoustic emission data clustering. *Compos Sci Technol* 2008;**68**:1258–65.